Volume 7 | Number 12 | 28 March 2016 | Pages 2153–2310

# Polymer Chemistry

www.rsc.org/polymers

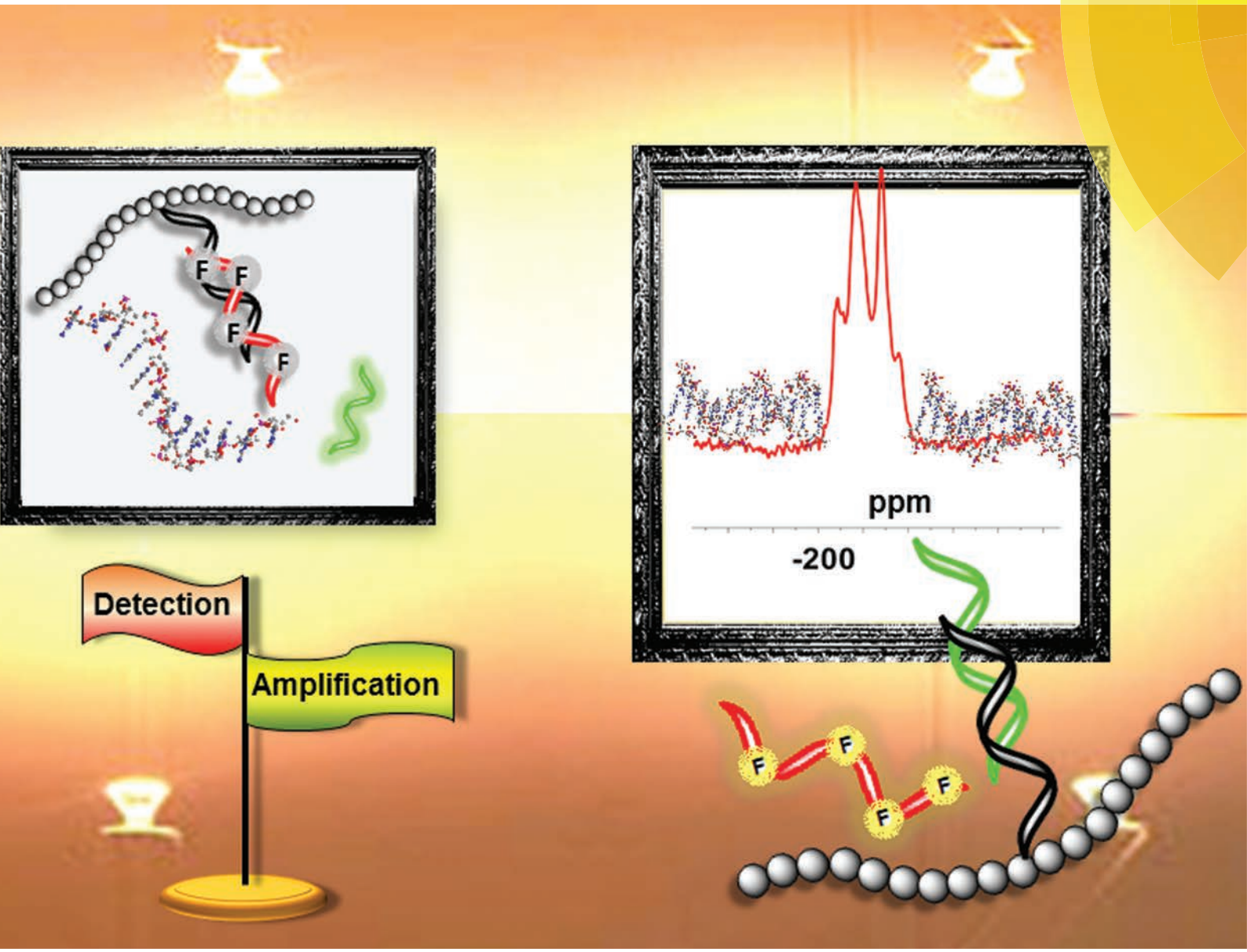


ISSN 1759-9954

ROYAL SOCIETY OF CHEMISTRY

PAPER

Giovanna Sicilia, Kristofer J. Thurecht, Cameron Alexander *et al.*
Synthesis of $^{19}F$ nucleic acid–polymer conjugates as real-time MRI probes of biorecognition

175 YEARS

Polymer Chemistry

PAPER

View Article Online
View Journal | View Issue



Cite this: *Polym. Chem.*, 2016, **7**, 2180

# Synthesis of $^{19}$F nucleic acid–polymer conjugates as real-time MRI probes of biorecognition†

Giovanna Sicilia,*[a] Adrienne L. Davis,[b] Sebastian G. Spain,[c] Johannes P. Magnusson,[a] Nathan R. B. Boase,[d,e] Kristofer J. Thurecht*[d,e] and Cameron Alexander*[a]

Received 26th November 2015,
Accepted 21st January 2016

DOI: 10.1039/c5py01883h

www.rsc.org/polymers

Polymer–DNA conjugates in which one nucleic acid strand contains fluorine-substituted nucleobases have been prepared and characterised. The efficacy of these novel $^{19}$F nucleic acid–polymer conjugates as sensitive and selective *in vitro* reporters of DNA binding events is demonstrated through a number of rapid-acquisition MR sequences. The conjugates respond readily and in a sequence specific manner to external target oligonucleotide sequences by changes in hybridisation. In turn, these structural changes in polymer–nucleotide conjugates translate into responses which are detectable in fluorine relaxation and diffusion switches, and which can be monitored by *in vitro* Spin Echo and DOSY NMR spectroscopy. Although complementary to conventional FRET methods, the excellent diagnostic properties of fluorine nuclei make this approach a versatile and sensitive probe of molecular structure and conformation in polymeric assemblies.

## Introduction

The ability of nucleic acids to recognize and hybridize with complementary sequences through highly specific base-pairing interactions underpins the basic function of biology, and, increasingly, is leading to a rich new field of synthetic functional materials.[1–4] In addition to well-explored themes in DNA 'origami',[5,6] applications of DNA-based materials and conjugates are emerging in molecular computation,[7] programmed synthesis,[8] drug delivery,[9,10] responsive hydrogels[11,12] and diagnostics.[13–15]

In the medical context, the potential for detecting specific nucleic acid sequences or changes in nucleobase interactions by magnetic resonance imaging (MRI) has attracted growing interest.[16,17] The *in vitro* and *in vivo* detection of therapeutically relevant oligonucleotide sequences represents an important step towards prevention or treatment of pathological processes. In attempts to produce nucleic acid based imaging agents capable of enhancing the sensitivity of the MRI technique, fluorine-labeled nucleotide building blocks[18] have recently been developed to exploit the excellent diagnostic properties exhibited by $^{19}$F nuclei, such as high natural abundance (100%), sensitivity (83% relative to $^{1}$H) and large gyromagnetic ratio (40.05 MHz T$^{-1}$, 94% relative to $^{1}$H).

Perhaps the most important features of the $^{19}$F nuclei as exogenous reporters are the sensitivities of the fluorine chemical shifts to changes in the local environment and the susceptibility of fluorine relaxation to molecular mobility.[19] The favorable spectroscopic properties of the $^{19}$F nucleus along with the lack of fluorine background signal in the body have encouraged chemists to synthesize fluorine-containing polymers for probing biological processes through the non-invasive techniques such as magnetic resonance imaging (MRI).

In order to be effective molecular imaging agents, $^{19}$F-labelled polymers have to embody design features such as high fluorine content, long spin–spin relaxation times ($T_2$) and short spin–lattice relaxation times ($T_1$). Among the wide range of fluorine-labelled polymers, a number of hyperbranched structures developed *via* controlled radical polymerization methods[20,21] have been investigated as $^{19}$F imaging reporters. The use of a branched polymeric structure coupled with random incorporation of fluorinated units within a hydrophilic PEG-based macrostructure ensures that the fluoro segments are always in a hydrated state and maintain high segmental mobility, which in turn lead to longer $^{19}$F $T_2$ and good *in vivo* MRI image quality.

Fluorine labelled nucleotide building blocks[18,22] have been synthesized in an attempt to monitor nucleic acid confor-

[a]*School of Pharmacy, University of Nottingham, University Park, Nottingham, NG7 2RD, UK*
[b]*School of Chemistry, University of Nottingham, University Park, Nottingham, NG7 2RD, UK. E-mail: cameron.alexander@nottingham.ac.uk, giovanna.sicilia@nottingham.ac.uk; Fax: +115 951 5122; Tel: +115 846 7678*
[c]*Department of Chemistry, Dainton Building; University of Sheffield, Sheffield, S3 7HF, UK*
[d]*Australian Institute for Bioengineering and Nanotechnology, The University of Queensland, St Lucia, Queensland 4072, Australia*
[e]*Centre for Advanced Imaging, The University of Queensland, St Lucia, Queensland 4072, Australia. E-mail: k.thurecht@uq.edu.au*
†Electronic supplementary information (ESI) available: Full experimental procedures and additional supporting figures. See DOI: 10.1039/c5py01883h

mational transitions consequent to metal ion binding,[23] ribozyme folding,[24] hairpin-duplex transitions[25] *via* 1D $^{19}$F NMR spectroscopy.

The elegant work of Mirkin *et al.*[26] is perhaps the first example of a smart fluorine-DNA based nanosensor that utilised fluorine labelled nucleic acids as *in vitro* MR reporters. In this system DNA strands functionalised with a tail of five 5-fluoro-uridines were hybridized to complementary DNA sequences immobilized on the surface of gold nanoparticles (AuNP). The close proximity of the $^{19}$F nucleobases to the AuNP surface decreased significantly the $^{19}$F NMR signal. In contrast, release of the $^{19}$F probes upon toehold-mediated strand displacement induced by target DNA strands resulted in a detectable fluorine peak.

Inspired by the work of Mirkin *et al.*, we embarked on a fundamental investigation of how molecular structure can be manipulated to influence the relaxation properties of the DNA probes. This was driven by the knowledge that although the presence of a single switchable $^{19}$F signal can be advantageous in the *in vitro* NMR detection of DNA binding events, it does not guarantee success of imaging *via* $^{19}$F MRI. Importantly, the relaxation of $^{19}$F nuclei plays an important role in magnetic resonance imaging and is a powerful parameter for manipulating $^{19}$F MR signals.

In this report a new example of $^{19}$F-nucleic acid polymer conjugate material is described. This polymer consists of a linear methacrylamide backbone functionalised with single stranded DNAs that act as anchors to graft partially complementary 2′-fluoro labelled oligonucleotides. The insertion of fluorine nuclei in the 2′ position of the ribose ring has been demonstrated to enhance the serum stability[27] and the binding affinity to RNA targets.[28] The choice of using a linear acrylic-type polymer was based on its ease of synthesis and functionalization through controlled radical polymerisation techniques. In the present work the aim was to demonstrate first the efficacy of a 2′-fluoro nucleic acid-polymer conjugate to respond in a sequence specific manner to external 'trigger' oligonucleotide sequences. The second aim was to translate such responses into detectable fluorine relaxation and diffusion switches that can be monitored by *in vitro* Spin Echo and DOSY NMR spectroscopy (Fig. 1), with potential for translation into an *in vivo* diagnostic through MR imaging.

## Experimental section

### Materials

Oligonucleotides A, C and D (HPLC purified, Table 1) were purchased from Biomers.net GmbH (Ulm, Germany) and used without further purification. DMT-2′Fluoro-dU phosphoramidite, DMT-2′Fluoro-dC(ac) phosphoramidite, DMT-2′Fluoro-dG (ib) phosphoramidite, DMT-2′Fluoro-dA(bz) phosphoramidite, DMT-dA(bz) phosphoramidite, DMT-dG(ib) phosphoramidite, DMT-dC(ac) phosphoramidite, DMT-dT phosphoramidite, CAP A (tetrahydrofura/pyridine/acetic anhydride, 8 : 1 : 1), CAP B (10% methylimidazole in tetrahydrofuran), TCA deblock (3% trichloroacetic acid in dichloromethane), methacrylamide (MAm, 98%), deuterium oxide 99.9% atom D ($D_2O$), Trizma® hydrochloride (Tris·HCl), *N*,*N*,*N*′,*N*′-tetramethylethylenediamine (TEMED, 99%), ammonium persulfate (APS, 98%), tris-borate-EDTA buffer (TBE, 10× concentrate), acrylamide/bis-acrylamide 29/1 (40% solution), triethylamine (TEA, >99%), methylene blue hydrate, methylamine solution (40 wt% in $H_2O$), sodium chloride (NaCl, 99%), trichloroacetic acid (TCA, ≥99%), ammonium hydroxide solution (28–30% $NH_3$ basis), ethylenediaminetetraacetic acid disodium salt

Table 1 Sequences and modifications of oligonucleotides used

| Name | 5′ | Sequence (5′–3′) |
|---|---|---|
| A | Aminohexyl | TAACAGGATTAGCAGAGCGAGG |
| A1 | Methacrylamidohexyl | TAACAGGATTAGCAGAGCGAGG |
| B1 | | CCUCGCTCUGCUAAUCC[a] |
| B2 | | CCUCGCUCUGCUAAUCC[a] |
| C | | CCTCGCTCTGCTAATCCTGTTA |
| D | | TTCAATCTCAACGGCTTCACCG |

[a] 2′-Fluoro modified nucleotides are underlined.

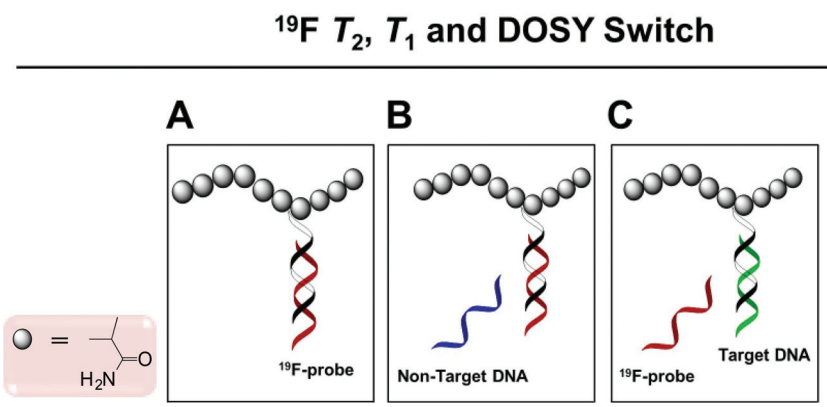


Fig. 1 Schematic illustration of the 2′-fluoro nucleic acid–polymer conjugate when free in solution (A), in presence of a non-specific (B) and a target DNA sequence (C).Interaction with external oligonucleotide sequences will result in distinctive $^{19}$F $T_2$, $T_1$ and DOSY changes.

dehydrate (EDTA), water BPC grade, DNase and RNase free, pentafluorophenyl methacrylate (PFPMA, 95%), Float-A-Lyzer® (MWCO 20 kDa) and Vivaspin 20 centrifugal concentrator (MWCO 10 kDa) were purchased from Sigma Aldrich. BTT activator (0.3 M 5-benzylthio-1-*H*-tetrazole in acetonitrile, anhydrous), Oxidiser (0.02 M iodine in tetrahydrofuran/pyridine/water, 89.6 : 0.4 : 10) and Ac-dC SynBase™ CPG 1000/110 were purchased from Link Technologies. 3-Hydroxypicolinic acid (3-HPA, ≥99%) and ammonium citrate dibasic (99%) were purchased from Fluka. OPC® Oligonucleotide Purification Cartridges were purchased from Applied Biosystems (Foster City, CA94404, USA). 2,2′-Azobis[2-(2-imidazolin-2-yl)propane]dihydrochloride (VA-044) was purchased from Wako Pure Chemical Industries. 10/60 Oligo length standard was purchased from Integrated DNA Technologies. All solvents were Fisher HPLC grade. All chemicals were used as received unless otherwise stated.

## Synthetic methods

### Synthesis and purification of 2′-fluoro oligonucleotides B1 and B2

*Automated synthesis.* The modified 2′-fluoro oligonucleotides B1 and B2 (Table 1) were synthesised on an Applied Biosynthesis 394 DNA/RNA automatic synthesiser at 1 μmol scale employing the standard solid phase β-cyanoethyl-phosphoramidite chemistry in trityl-on mode.[29] The synthesis occurred from the 3′ towards the 5′ end of the oligonucleotide strands on pre-packed Ac-dC SynBase™ CPG 1000/110 solid phase columns. 0.1 M solution in dry acetonitrile of DMT-2′-fluoro dU, DMT-2′-fluoro dA(bz), DMT-2′fluoro dG(ib), DMT-2′-fluoro dC(ac) phosphoramidites and standard DNA phosphoramidites such as DMT-dT, DMT-dA(bz), DMT-dG(ib), DMT-dC(ac) were used in the synthesis of the $^{19}$F probes B1 and B2. Extended coupling times of 5 min were used for the base condensation of both fluorinated and non-fluorinated phosphoramidites.

*Ultrafast deprotection (general procedure for 1 μmol scale synthesis).* Cleavage of the trityl-on 2′-fluoro modified oligonucleotides from the solid support and base de-protection was achieved by treatment with 2 mL of a 1 : 1 mixture (v/v) of aqueous ammonium hydroxide solution (28–30% w/v) and aqueous methylamine (40% w/v). The mixture was reacted for 10 min at 20 °C. Afterwards, the reaction mixture was heated to 65 °C for 30 min. Finally, the solution was diluted with 2 mL of water BPC grade and purified by OPC® cartridges.

*OPC® oligonucleotide cartridge purification (general procedure for 1 μmol scale synthesis).* Detritylation and purification of the trityl-on oligonucleotides B1 and B2 were performed *via* OPC® oligonucleotide cartridge purification following a standard procedure provided from the supplier Applied Biosystems (Foster City, CA, USA) with modifications. Briefly, an OPC® cartridge was connected to a polypropylene syringe and flushed with acetonitrile HPLC grade (5 mL) and 2 M triethylammonium acetate (5 mL). The solution containing the oligonucleotide was passed through the OPC® cartridge at a rate of 1 drop per second. The eluate was collected and passed through the cartridge a second time. Afterwards, the system was flushed with 1.5 M ammonium hydroxide (5 mL), followed by water (BPC grade DNase-Rnase free, 10 mL). 3% Trichloroacetic acid in water (5 mL) was slowly passed through the OPC® cartridge to waste to effect detritylation. The cartridge was flushed with water (10 mL) and the detritylated oligonucleotide was collected by gently passing 20% (v/v) acetonitrile (2 mL).

The pure 2′-fluoro modified oligonucleotides B1 and B2 were analysed by rp-HPLC and MALDI-TOF mass spectrometry. B1: $M_{calc}$ = 5073.2 Da; $M_{found}$ = 5130.2 Da; B2: $M_{calc.}$ = 5275 Da; $M_{found}$ = 5353.1 Da.

**Synthesis of 5′-methacrylamidyl oligonucleotide A1 (MAmA1).** 5′-Amino modified oligonucleotide A (19 nmol, Table 1) was dissolved in water (30 μL, BPC grade). DIPEA (1 μL, 5.7 μmol) was added and the mixture was stirred for five minutes at room temperature. Pentafluorophenyl methacrylate (2 μL, 11 μmol) was dissolved in anhydrous DMSO (23 μL) and 2.3 μL of the resulting solution was added to the DNA solution. The reaction was allowed to proceed overnight at 20 °C. The crude product was purified by reverse-phase HPLC and analyzed by MALDI-TOF mass spectrometry (Fig. S1†). DNA A1: $M_{calc}$ = 7106 Da, $M_{found}$ = 7108.1 Da.

**Synthesis *via* RAFT polymerisation of poly(methacrylamide-*co*-methacrylamidyl oligonucleotide A1) [p(MAm-*c*-MAmA1)].** Methacrylamide (MAm) (647 mg, $7.6 \times 10^{-3}$ mol, 120 eq.), 5′-methacrylamidyl oligonucleotide A1 (MAmA1) (52 mg, $7.3 \times 10^{-6}$ mol, 0.1 eq.) in $D_2O$ (3 mL), 2-(2-hydroxyethylthiocarbonothioylthio)-2-methylpropionic acid (15.1 mg, $6.3 \times 10^{-5}$ mol, 1 eq.) in $D_2O$ (12.4 mL) and VA-044 (6.1 mg, $1.9 \times 10^{-5}$ mol, 0.3 eq.) in $D_2O$ (0.4 mL) were mixed together in a round bottom flask equipped with a magnetic stirrer bar and sealed with a rubber septum and parafilm. The solution was degassed under nitrogen stream for 30 min, followed by immersion in an oil bath preheated to 50 °C. After 8 h a gel-like precipitate was visible in the reaction mixture. At regular time intervals (10 h, 20 h, 30 h and 44 h), aliquots (50 μL) were removed for HPLC kinetic studies and 0.15 eq. of VA-044 (3.1 mg, $9.5 \times 10^{-6}$ mol) in $D_2O$ (0.2 mL) was added to the reaction mixture under nitrogen flow. After 56 h, the polymerization was quenched by placing the flask in an ice bath and exposing to air for 5 min. The reaction mixture was centrifuged at 5000 rpm for 15 min to separate the liquid phase from the gel-like precipitate. The supernatant was dialysed against water for 60 h using a Float-A-Lyzer® (MWCO 20 kDa) and subsequently purified *via* anion exchange HPLC to remove traces of unreacted oligonucleotide A1. The pure polymer was desalted using Vivaspin®20 (MWCO 10 kDa) and analysed *via* $^1$H NMR, GPC, DLS.

$^1$H NMR: (400 MHz; 50 mM NaCl, 10 mM Tris·HCl, 1 mM EDTA in $D_2O$, pH 7.5) $\delta$ (ppm) 8.4–6.6 (*m*, 8H of adenine and guanine; 2H of adenine; 6H of cytosine and thymine); 6.3–5.3 (m, 5H of cytosine; 1′H of deoxyribose); 4.5–3.7 (m, 4′H, 5′H, 5″H of deoxyribose);3.9 (s, –$CH_2$ of EDTA); 3.7 (s, –$CH_2$ of Tris); 3.6 (s, –$CH_2$ of EDTA); 2.8–1.6 (br m, $CH_2$ polymer backbone; 2′H,2″H of deoxyribose); 1.6–0.5 (br s, $CH_3$ of polymer backbone; $CH_3$ of thymine).

 

GPC: $M_n$ = 27.4, $M_w$ = 32.3, $Đ$ = 1.18.

DLS: Intensity distribution $R_h$ = 6.7 ± 2.7 nm.

**Synthesis of poly(methacrylamide-*co*-methacrylamidyl oligonucleotide A1B2) [p(MAm-*c*-MAmA1B2)].** 2′-Fluoro oligonucleotide B2 and p(MAm-*c*-MAmA1) were mixed at a DNA mole ratio of 1/1.3 respectively in annealing buffer (10 mM Tris·HCl, 50 mM NaCl and 1 mM EDTA pH = 7.5) at a final concentration of 2.5 mM. The mixture was heated at 95 °C for 20 min and then left to cool for 50 min.

## Analytical methods

**Nuclear magnetic resonance spectroscopy (NMR).** All NMR experiments were carried out at 298 K on a Bruker AV400 spectrometer fitted with a 5 mm auto-tunable broad-band (BBFO) probe. Samples were dissolved in 700 μL of $D_2O$ containing 10 mM Tris·HCl, 50 mM NaCl and 1 mM EDTA (pH 7.5) at the following concentrations: B2, 1.1 mM; p(MAm-*c*-MAmA1), 1.4 mM; p(MAm-*c*-MAmA1B2), 2.5 mM; p(MAm-*c*-MAmA1B2) + C, 3.5 mM, p(MAm-*c*-MAmA1B2) + D, 5.7 mM. Spectra were analysed with MestReNova 6.2 and TopSpin 2.1.

Oligonucleotide $^1$H NMR assignments were performed according to the $^1$H NMR chemical shift ranges described by Wüthrich[30] for single stranded and duplex DNA and RNA fragments.

**$^1$H NMR $T_2$ and $T_1$ measurements.** 1D $^1$H NMR spectra were acquired at 400.13 MHz using $D_2O$ as an internal lock. A 90° pulse of 14 μs was applied in all measurements. The relaxation delay was 1 s and the acquisition time was 2 s. Data were collected using a spectral width of 8 kHz, 33k data points and 16 scans.

**$^1$H spin–spin relaxation times ($T_2$)** were measured using the Carr–Purcell–Meiboom–Gill (CPMG) pulse sequence.[31] Depending on the sample analysed, the relaxation delay was either 10 or 15 s and the acquisition time was 1.9 s. For each measurement, the echo times were from 1.6 ms to 417 ms and 12–16 points were collected (Table S2†).

**$^1$H spin–lattice relaxation times ($T_1$)** were measured using the standard inversion-recovery pulse sequence.[31] The relaxation delay was either 12 or 16 s and the acquisition time was 1.9 s. For each measurement, the recovery times were from 4 ms to 12 s or 18 s and 10–12 points were collected (Table S3†).

**$^{19}$F NMR $T_2$ and $T_1$ measurements.** 1D $^{19}$F NMR spectra were acquired at 376.5 MHz without $^1$H decoupling. A 90° pulse of 31 μs was applied in all measurements, the relaxation delay was 3 s and the acquisition time was 1.7 s. Data were collected using a spectral width of 19 kHz, 65k data points and 64–256 scans.

**$^{19}$F spin–spin relaxation times ($T_2$)** were measured using the CPMG pulse sequence.[31] The relaxation delay was either 3 s or 4 s and the acquisition time was 1.9 s. For each measurement, the echo times were from 4.1 ms to 74.2 ms and 14 points were collected (Table S4†). In order to reduce the possibility of sample heating during $^{19}$F $T_2$ relaxation experiments, the power of the $^{19}$F pulses was reduced below the maximum level at all times. Pulses were applied close to, or on, resonance.

**$^{19}$F spin–lattice relaxation times ($T_1$)** were measured using the standard inversion-recovery pulse sequence. The relaxation delay was either 2.5 s or 5 s and the acquisition time was 1.7 s. For each measurement, the recovery times were from 4 ms to 5 s and 9–16 points were collected (Table S5†).

**$^1$H and $^{19}$F $T_2$, $T_1$ curve fitting.** Spin–spin ($T_2$) and spin–lattice ($T_1$) relaxation times of $^1$H and $^{19}$F nuclei were described either by single exponential functions or by the sum of two exponential relaxation decays when short and long decay rates were present.[31,32] $T_2$ and $T_1$ decay curves were analysed with SigmaPlot version 10.0, from Systat Software, Inc., San Jose, California, USA (Table S6†). Accordingly, for single exponential decay rates $T_1$ and $T_2$ were calculated using eqn (S1).† For double exponential decay rates $T_1^{Short}$, $T_2^{Short}$, $T_1^{Long}$ and $T_2^{Long}$ were calculated using eqn (S2) and (S3).†

**Measurement of self-diffusion coefficients. $^1$H diffusion experiments** were carried out using a stimulated echo sequence employing bipolar gradient pulse pairs[33–35] (the standard Bruker AU program *ledbpgppr2s*). Presaturation was employed during the relaxation delay for water suppression. For each FID, 16 scans were collected with 5 s relaxation delays; 32k data points were collected and 8 or 16 experiments were acquired at increasing gradient strengths covering a spectral width of 20 ppm. Prior to Fourier transformation, exponential multiplication was applied with 2 or 5 Hz line broadening. The diffusion time ($\Delta$) and the gradient length ($\delta$) were set to 200 ms and 5 ms respectively, while the recovery delay after gradient pulses ($\tau$) was 200 μs.

**$^{19}$F diffusion experiments** were carried out using the standard Bruker pulse program *ledbpgp2s*. The pulse program applied stimulated echoes using bipolar gradient pulses for diffusion and 2 spoil gradients.[34,35] For each FID, 1024 scans were collected with 4 s relaxation delays; 32k data points were collected and 8 experiments were acquired at increasing gradient strengths. Prior to Fourier transformation exponential multiplication was applied with 50 or 150 Hz line broadening. The diffusion time ($\Delta$) and the gradient length were set to 200 and 5 ms respectively, while the recovery delay ($\tau$) after gradient pulses was 5 ms.

In order to minimise convection effects, the VT air flows in the probe were increased to 535 L h$^{-1}$ in all diffusion experiments.

*$^1$H and $^{19}$F diffusion curve fitting.* The integrals of selected regions in the 1D $^1$H and $^{19}$F spectra were measured at different gradient strengths and fitted to the eqn (S5)–(S8).†[34]

*2D $^1$H DOSY spectra.* 2D $^1$H diffusion spectra were elaborated with the DOSY module of Bruker's TopSpin 2.1 selecting as processing method "exponential", two fitting components and a line broadening factor of 3.0.

**Strand displacement experiments**

*PAGE assay.* The hybrid p(MAm-*c*-MAmA1B2) was combined with 1 or 2 mole equiv. of either complementary (strand C) or scrambled (strand D) DNA in annealing buffer at a final concentration of 90–117 μM. Samples were incubated for 30 min

at room temperature and then analysed by native PAGE as previously described.

*NMR assay.* The NMR sample containing the hybrid p(MAm-*c*-MAmA1B2) (2.5 mM) in 700 μL of deuterated annealing buffer (50 mM NaCl, 10 mM Tris·HCl and 1 mM EDTA in $D_2O$, pH 7.5) was used to dissolve either 1 mole equiv. of the complementary (strand C) or scrambled (strand D) DNA affording a final concentration of 3.6 mM. Specifically, 200 μL of p(MAm-*c*-MAmA1B2) were transferred with a 200 μL micropipette fitted with sterile tips from a glass NMR tube (5 mm) to a centrifuge tube containing lyophilised strand C or D. The solution was mixed and transferred back to the NMR tube. The samples, p(MAm-*c*-MAmA1B2) + C and p(MAm-*c*-MAmA1B2) + D, were incubated for 30 min at room temperature and then analysed by NMR.

This process was repeated for p(MAm-*c*-MAmA1B2) + D to incorporate additional amounts of strand D (2 mole equiv.) and strand C (5 mole equiv.).

## Results and discussion

### Design, synthesis and $^{19}$F relaxation analysis of 2′-fluoro modified oligonucleotides B1 and B2

Two 17-*mer* 2′-fluoro-modified oligonucleotide sequences B1 and B2 were synthesised *via* automated solid-phase chemistry using commercially available DMT-2′-deoxy and DMT-2′-fluoro modified phosphoramidites as building blocks. The synthesis of both oligonucleotides gave satisfactory yields with ~95% coupling efficiency. As shown in Table 1, B1 contained 4 2′-fluoro-uridines whereas B2 consisted of 16 2′-fluoro nucleotides.

Fast deprotection of the 2′-fluoro containing oligonucleotides was achieved by treatment with aqueous methylamine and ammonium hydroxide at 55 °C for 30 min. Detritylation and removal of failure sequences from the full length products were performed *via* OPC® oligonucleotide cartridge purification. The purity of the 2′-fluoro modified oligonucleotides B1 and B2, was confirmed by MALDI-TOF mass spectrometry and rp-HPLC (Fig. S2†).

The presence of a different number of fluorinated units within the oligonucleotides B1 and B2 provided a useful handle to investigate the effects of fluorine content on the relaxation properties of both strands. The higher fluorine content in B2 resulted in a broad $^{19}$F signal (Fig. 2A) with shorter $T_2$ and $T_1$ relaxation times (Fig. 2B–D). These effects arose due to the enhanced chemical shift anisotropy and dipole–dipole coupling to near neighbour fluorine and proton spins induced by the insertion of more fluorine nuclei as has been previously observed in polymeric $^{19}$F probes.[36]

Moreover, the $^{19}$F transverse and longitudinal relaxations in both oligonucleotides B1 and B2 were characterised by a bi-exponential decay indicative of the existence of two populations of fluorine spins experiencing different local mobility.[37] As

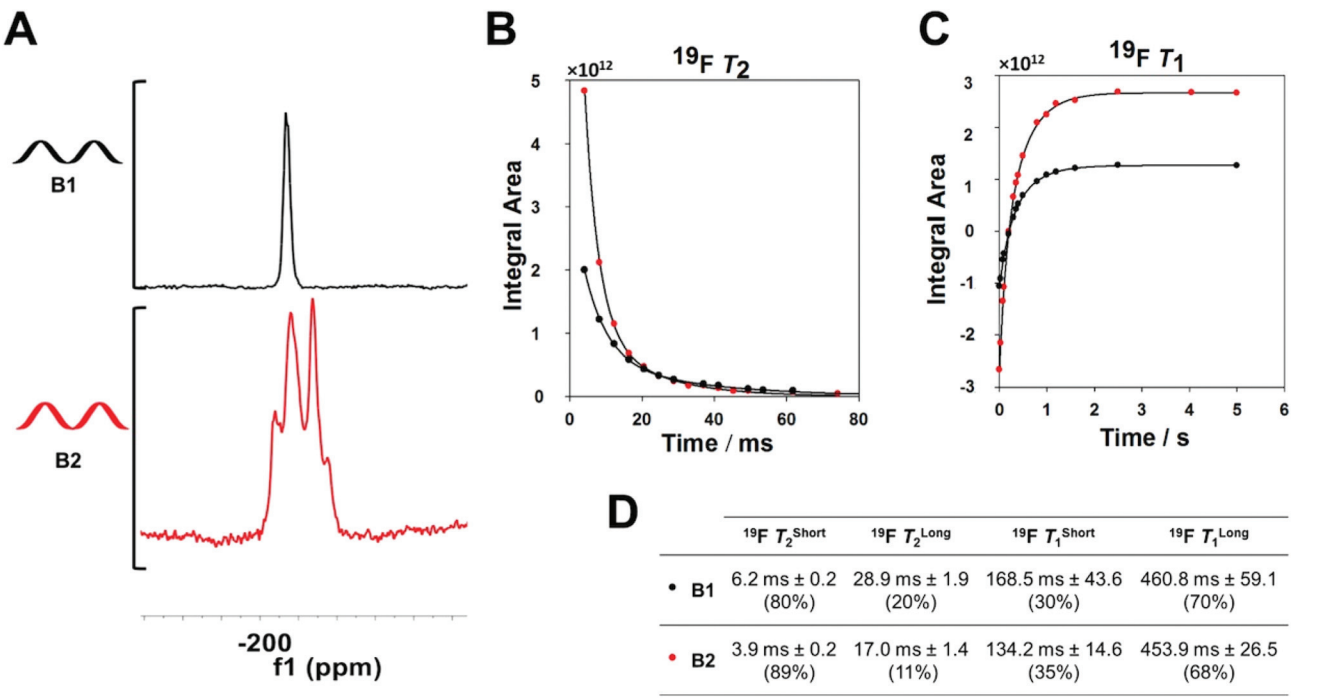


D

| | $^{19}$F $T_2^{Short}$ | $^{19}$F $T_2^{Long}$ | $^{19}$F $T_1^{Short}$ | $^{19}$F $T_1^{Long}$ |
|---|---|---|---|---|
| • B1 | 6.2 ms ± 0.2 (80%) | 28.9 ms ± 1.9 (20%) | 168.5 ms ± 43.6 (30%) | 460.8 ms ± 59.1 (70%) |
| • B2 | 3.9 ms ± 0.2 (89%) | 17.0 ms ± 1.4 (11%) | 134.2 ms ± 14.6 (35%) | 453.9 ms ± 26.5 (68%) |

**Fig. 2** (A) 1D $^{19}$F NMR of oligonucleotides B1 (black) and B2 (red) in $D_2O$ containing 50 mM NaCl, 10 mM Tris·HCl, 2 mM EDTA pH 7.5. (B) $^{19}$F spin–spin ($T_2$) relaxation times measurements for oligonucleotide B1 (black circles) and oligonucleotide B2 (red circles) fitted with biexponential decay curves. (C) $^{19}$F spin–lattice ($T_1$) relaxation times measurements of oligonucleotide B1 (black circles) and B2 (red circles) fitted with biexponential decay curves. (D) List of short and long $^{19}$F $T_2$ and $^{19}$F $T_1$ relaxation times with relative standard error and abundance (%) measured for oligonucleotides B1 and B2.

 

described by Pearson[38] and Xiao,[39] the insertion of fluorine in organic and or biologically relevant molecules can induce local structural changes due to the enhanced solvophobic interactions introduced by the fluorine atoms. These interactions are strong and can significantly affect the local organisation of the fluorinated moieties leading to localised aggregation.

As noted above, the attractive interactions between fluorine atoms promoted aggregation of the oligonucleotide strands.

The electrophoretic migration of B1 and B2 along a 30% native PAGE was characterised by two separate bands (Fig. S3†). By comparison with a DNA standard comprising a set of eight oligonucleotide fragments of different length ranging from 10 to 60 base pairs, it could be observed that part of the B1 and B2 strands were migrating at the same rate as 30 and 40 base pair oligonucleotides. Therefore, from the PAGE analysis we hypothesise that the fast spin–spin ($T_2$s) and spin–lattice relaxation times ($T_1$s) arose from fluorine nuclei of aggregated strands experiencing restricted mobility while the long $T_2$s and $T_1$s involved fluorine nuclei of less entangled strands encountering higher mobility.

### Oligonucleotide B2 as a strand of choice

In order to be imaged successfully, a $^{19}$F tracking agent needs to display high signal intensity, high fluorine content, long spin–spin relaxation times ($T_2$) and short spin–lattice relaxation times ($T_1$).[40]

As shown in Fig. 2D, ~70% of the total fluorine spins of the 2′-fluoro modified oligonucleotides B1 and B2 displayed sufficiently short spin–lattice relaxation times with $T_1s^{Long}$ of 460.8 ms and 453.9 ms respectively, such that experiments could be conducted within a useful timeframe. In contrast, the $T_2$s measured for both strands were close to the detection limit of the MRI technique, leading to a decrease in intensity of the measured samples. More than 80% of the fluorine spins of both B1 and B2 were characterised by fast spin–spin relaxation processes with $T_2^{Short}$ values in the range of 6.2 and 3.9 ms respectively.

The data discussed refers only to the $T_2^{Short}$ and $T_1^{Long}$ values as these are the populations that gave a significant contribution to the fluorine spin–spin and spin–lattice relaxation processes in both oligonucleotide B1 and B2.

Considering the similarity between probes, in the present study oligonucleotide B2 was selected as a model $^{19}$F probe due to its higher fluorine content that could guarantee a stronger signal to noise ratio during the *in vitro* NMR acquisitions.

### $^1$H spin–spin and spin–lattice relaxation of oligonucleotide B2

In order to gain more information about the relationship between relaxation rates and structural features of the fluorine-labelled probe B2, $^1$H spin relaxations were analysed. $^1$H spin–spin and spin–lattice relaxations were evaluated only for proton nuclei resonating at 8.5–7.6 ppm and 6.4–5.5 ppm due to their distance from the strong water peak in the spectrum that confounds analysis of neighbouring peaks (Fig. S4†). In contrast to the $^{19}$F nuclei, the observed $^1$H spins displayed longer $T_2$ (120.5–116.3 ms) and $T_1$ (1.68 s) relaxation times. This effect can be explained by consideration of the relaxation mechanisms that govern $^1$H and $^{19}$F nuclei. Both spins relax *via* dipole–dipole coupling to near neighbour nuclei. However, $^{19}$F spins receive an additional contribution to relaxation from the chemical shift anisotropy that promotes transverse and longitudinal relaxation resulting in shorter $T_2$ and $T_1$ values.[41] Moreover, $^1$H spin–spin ($T_2$) and spin–lattice ($T_1$) relaxations exhibited single exponential decay rates. This effect was possibly a consequence of the different position occupied by $^1$H and $^{19}$F spins within the nucleotides of the B2 strand. Protons resonating at 8.5–7.6 ppm and 6.4–5.5 ppm were located on the nucleobases and therefore distant enough from the sugar ring containing the fluorine nuclei to be influenced by the local mobility changes occurring in the vicinity of the fluorine spins. Finally, the spin–spin relaxation times observed for $^1$H resonating at 8.5–7.6 ppm and 6.4–5.5 ppm ($T_2$s of 120.5 and 116.3 ms, Fig. S4†) were 13–14 fold lower than the relative spin–lattice relaxation times ($T_1$ = 1.68 s). Longitudinal relaxation occurs in presence of local magnetic fields that fluctuate at the Larmor frequency of the observed nuclear spin. Large molecules tumble slowly in solution generating local magnetic fields that fluctuate at a rate that does not allow spin–lattice relaxation and therefore resulting in long $T_1$ relaxation times. However, the slow tumbling rate of large molecules is capable of favouring spin–spin relaxation due to the sensitivity of $T_2$ to low frequency fluctuations.[31]

### $^1$H and $^{19}$F diffusion analysis of oligonucleotide B2

$^1$H and $^{19}$F diffusion ordered spectroscopy experiments were carried out to gain information on the molecular dynamics of the 2′-fluoro modified oligonucleotide B2 in solution, and to provide confirmation of molecular structure. As shown in Fig. S5,† $^1$H resonating at 8.5–7.6 ppm and 6.4–5.5 ppm and $^{19}$F spins displayed similar self-diffusion coefficients in the range of $5.2 \times 10^{-9}$ and $5.8 \times 10^{-9}$ m$^2$ s$^{-1}$ demonstrating that all the nuclei analysed were part of the same molecular structure.

### Synthesis and characterisation of p(MAm-c-MAmA1)

In order to introduce the nucleic acid functionality into a linear polymeric platform, polymerizable DNA strand A1 (Table 1) was synthesised by reacting 5′-amino oligonucleotide A (Table 1) with pentafluorophenyl methacrylate. The strand A1 was characterised by a 17-*mer* sequence complementary to the fluorine labelled probe B2 and a 5-base overhang to enable strand displacement by a target oligonucleotide sequence. The linear copolymer p(MAm-*c*-MAmA1) was synthesised *via* a RAFT technique. 5′-Methacrylamidyl DNA A1 (MAmA1) was copolymerised with methacrylamide (MAm) in water at 50 °C using 2-(2-hydroxyethylthiocarbonothioylthio)-2-methylpropionic acid and VA-044 as RAFT chain transfer agent (CTA) and initiator respectively (Fig. S6†).

The above mentioned reagents were mixed to obtain a final molar ratio of 120 : 0.1 : 1 : 0.3 (MAm : MAmA1 : CTA : VA-044). The molar concentration of 5′-methacrylamidyl oligonucleotide A1 was kept lower than the methacrylamide

monomer in an attempt to balance the length of the polymer backbone and the oligonucleotide side chains. Moreover, the low degree of DNA functionalization per polymer chain was considered to be advantageous as it would reduce the steric hindrance in the following hybridization step, making the strand A1 more accessible to the fluorinated probe B2.

Because of its short half-life of 10 h at 40 °C, 0.15 eq. of VA-044 was added to the reaction mixture every 10 h for 40 h in order to keep constant the source of radicals. After 8 h, a gel like precipitate was visible in the reaction chamber. The gel consisted of only methacrylamide as shown by the 1D $^1$H NMR acquired after gel solubilisation in $D_2O$ (Fig. S7†). No trace of MAmA1 could be detected by $^1$H NMR and UV-vis spectroscopy. This gave an insight into the kinetics of the polymerization progress with MAm reacting faster than MAmA1 due to its less bulky structure. The consumption of MAmA1 during the polymerisation was monitored *via* anion exchange HPLC. As shown in Fig. S8,† 58% of MAmA1 reacted after 44 h. As the polymerisation rate of MAmA1 became very slow in the following hours, the reaction was stopped after 56 h when 59% of the initial oligonucleotide A1 was polymerised.

The reaction mixture was first dialysed against water for 60 h with MW cut off of 20 kDa, however unreacted MAmA1 remained. Consequently, it was then purified *via* anion exchange HPLC to remove the unreacted 5′-methacrylamidyl oligonucleotide A1.

The final copolymer composition was calculated from the $^1$H NMR acquired on the pure polymer by comparing the integrals of the protons of MAm (5H, $-CH_2$ and $-CH_3$ per monomer unit) and MAmA1 [5H,$-CH_2$ and $-CH_3$; 30H, DNA A1 (signals between 8.5–6.9 ppm] (for details see ESI, Fig. S9 and eqn (S5)–(S7)†). As part of the initial fraction of methacrylamide was lost in the formed gel, the final composition percentage of MAm (~99.6%) was slightly lower than the target value (~99.9%, Fig. S9†).

The pure polymer was characterised by aqueous phase GPC and DLS. As shown in Fig. S9,† p(MAm-*c*-MAmA1) displayed an $M_n$ of 27.4 kDa and a $Đ$ of 1.18. The DLS intensity distribution showed one population with $R_h \sim 6.7$ nm (Fig. S10†).

### $^1$H spin–spin and spin–lattice relaxation analysis of p(MAm-*c*-MAmA1)

As described for oligonucleotide B2, spin–spin ($T_2$) and spin–lattice ($T_1$) relaxation times were measured for proton nuclei resonating in region of the 1D $^1$H NMR spectrum distant from the water peak (Fig. S11†). Therefore, $^1$H $T_2$ and $^1$H $T_1$ relaxation processes were investigated for protons belonging to the methyl side chain ($CH_3$, 1.4–0.8 ppm) the methylene groups ($CH_2$) constituting the polymer backbone (2.0–1.6 ppm) and the nucleobases of the oligonucleotide A1 (8.5–7.6 ppm and 6.4–5.5 ppm).

All the $^1$H $T_2$ measured displayed biexponential decay rates with two populations of $^1$H $T_2$s. As shown in Fig. S10,† the long $T_2$ component was dominant (≥52%) for the oligonucleotide protons resonating at 8.5–7.6 ppm ($T_2^{Long}$ = 114.9 ms) and 6.4–5.5 ppm ($T_2^{Long}$ = 57.1 ms), whereas the short $T_2$ component was dominant (≥77%) for the methylene ($T_2^{Short}$ = 2.5 ms) and methyl groups ($T_2^{Short}$ = 2.9 ms). These observations were indicative of the fact that the protons belonging to the long side chain represented by the oligonucleotide A1 were experiencing a different local mobility from the protons constituting the polymer backbone ($CH_2$ groups) and the methyl side chains. The $^1$H $T_2$ is mainly influenced by the dipole–dipole interactions of nuclear spins. As described by Claridge *et al.*,[31] the proton dipolar relaxation mechanism has a strong distance dependence and is affected by the motion of the polymer chain. Here, the short inter-nuclear distances between the proton of the methylene and methyl groups and the slow tumbling rate along the polymer backbone enhanced the dipole–dipole relaxation and hence promoted faster spin–spin relaxation processes that resulted in two broad signals in the 1D $^1$H NMR spectrum (Fig. S11†). In contrast, the higher internuclear distance between the protons located on the nucleobases resulted in longer spin–spin relaxation times.

Moreover, the different molecular mobility of the analysed protons also had notable effects on the $^1$H spin–lattice relaxations ($T_1$). The oligonucleotide protons resonating at 8.5–7.6 ppm and 6.4–5.5 ppm were characterised by long $T_1$s in the range of 1.7–1.8 s. In contrast, the proton of methylene and methyl groups forming the polymer backbone were characterised by fast spin–lattice relaxation processes with $T_1$ values in the range of 652.8–631.6 ms.

### $^1$H diffusion analysis of p(MAm-*c*-MAmA1)

$^1$H nuclei resonating at 8.5–7.6 ppm, 6.4–5.5 ppm, 2.0–1.6 ppm and 1.4–0.8 ppm displayed similar self-diffusion coefficients in the range of 6.4–6.7 × $10^{-10}$ $m^2$ $s^{-1}$ (Fig. S12†).

These data indicated that the entire polymer chains, with and without DNA A1, were diffusing at the same rate. These results were in agreement with the GPC and DLS data and hence gave further confirmation of the low-dispersity of p(MAm-*c*-MAmA1).

### Synthesis of p(MAm-*c*-MAmA1B2)

The poly(methacrylamide-*co*-methacrylamidyl oligonucleotide A1B2) [p(MAm-*c*-MAmA1B2)] was produced by hybridization of the 2′-fluoro modified strand B2 to the nucleic acid functionality A1 of p(MAm-*c*-MAmA1) under standard conditions.

The oligonucleotide annealing ratio was screened *via* PAGE analysis. As shown in Fig. S13,† B2 and p(MAm-*c*-MAmA1) were annealed at different DNA molar ratios of 1 : 1.3, 1 : 1.5 and 1 : 2 respectively. The electrophoretic migration along a 20% native PAGE revealed the presence of traces of unbound strand B2 (Fig. S13,† dashed rectangle) in all the ratios screened. Because the traces of unbound B2 resulted in bands of similar intensity in all the samples analysed, the lower annealing ratio of 1 : 1.3 (B2: p(MAm-*c*-MAmA1) was selected as the standard experimental ratio in the present study. Since the presence of a small amount of unbound B2 was considered to have negligible effects in the

 

subsequent investigations, the hybrid p(MAm-*c*-MAmA1B2) was used without further purification.

### $^{19}$F $T_2$ and $T_1$ relaxation of p(MAm-*c*-MAmA1B2)

The hybridization of the B2 strand to p(MAm-*c*-MAmA1) was accompanied by evident effects on the fluorine signal shape. As shown in Fig. 3A (black trace), a sharper $^{19}$F signal, shifted slightly downfield, appeared when the B2 strand was bound to p(MAm-*c*-MAmA1). This effect was also observed by Kiviniemi *et al.*[42] in the analysis of fluorinated PNAs. When the PNAs decorated with 3 or 9 $^{19}$F nuclei were bound to anti-parallel or parallel DNAs or RNAs a sharper signal appeared in the $^{19}$F spectrum. Kiviniemi inferred the change in peak shape to the formation of a more defined structure consequent to the hybridization of complementary oligonucleotides. This highlights the sensitivity of $^{19}$F nuclei to neighbouring groups, and also the potential to extract far more information from acquired $^{19}$F NMR spectra than just a change in intensity of the peak following a switch. However, the hybridization of the 2′-fluoro modified strand B2 to p(MAm-*c*-MAmA1) did not cause any significant changes in the $^{19}$F spin–spin ($T_2$) relaxation times (Fig. 3B). In contrast, notable changes could be observed in the longitudinal relaxation times $T_1$. By comparison with the oligonucleotide B2, 88% of the total fluorine spins of the hybrid p(MAm-*c*-MAmA1B2) displayed a longer spin–lattice relaxation time of ~513 ms (Fig. 3C and D), providing a potential mechanism for probing molecular hybridization changes through monitoring T1.

### $^{1}$H $T_2$ and $T_1$ relaxation analysis of p(MAm-*c*-MAmA1B2)

$^{1}$H $T_2$ and $T_1$ relaxation times and relative decay curves were analysed for protons belonging to the methyl side chains ($CH_3$, 1.16–1.08 ppm) constituting the polymer backbone and the protons located on the nucleobases of the oligonucleotide duplex A1B2 (Fig. S14†).

Comparing the $^{1}$H $T_2$ relaxation times of the hybrid p(MAm-*c*-MAmA1B2) with the fluoro labelled probe B2 when free in solution, significant changes could be observed for the oligonucleotide protons. Specifically, the $^{1}$H $T_2$ decreased to about 72 ms and 87 ms for protons resonating at 8.5–7.6 ppm and 6.4–5.5 ppm respectively. These results were a direct consequence of conformational changes in the oligonucleotide strands, with restricted molecular motion induced by the formation of a more rigid double helix structure enhancing the $^{1}$H spin–spin relaxation ($T_2$).

In contrast, the protons of methyl side chains did not undergo any significant change, displaying values in the same range as those observed for p(MAm-*c*-MAmA1) (Fig. S13†). These results were in agreement with the values expected as the major relaxation changes should only affect the oligonucleotide protons during the hybridization process.

The binding of B2 to p(MAm-*c*-MAmA1) influenced also the longitudinal relaxation times of the oligonucleotide $^{1}$H spins

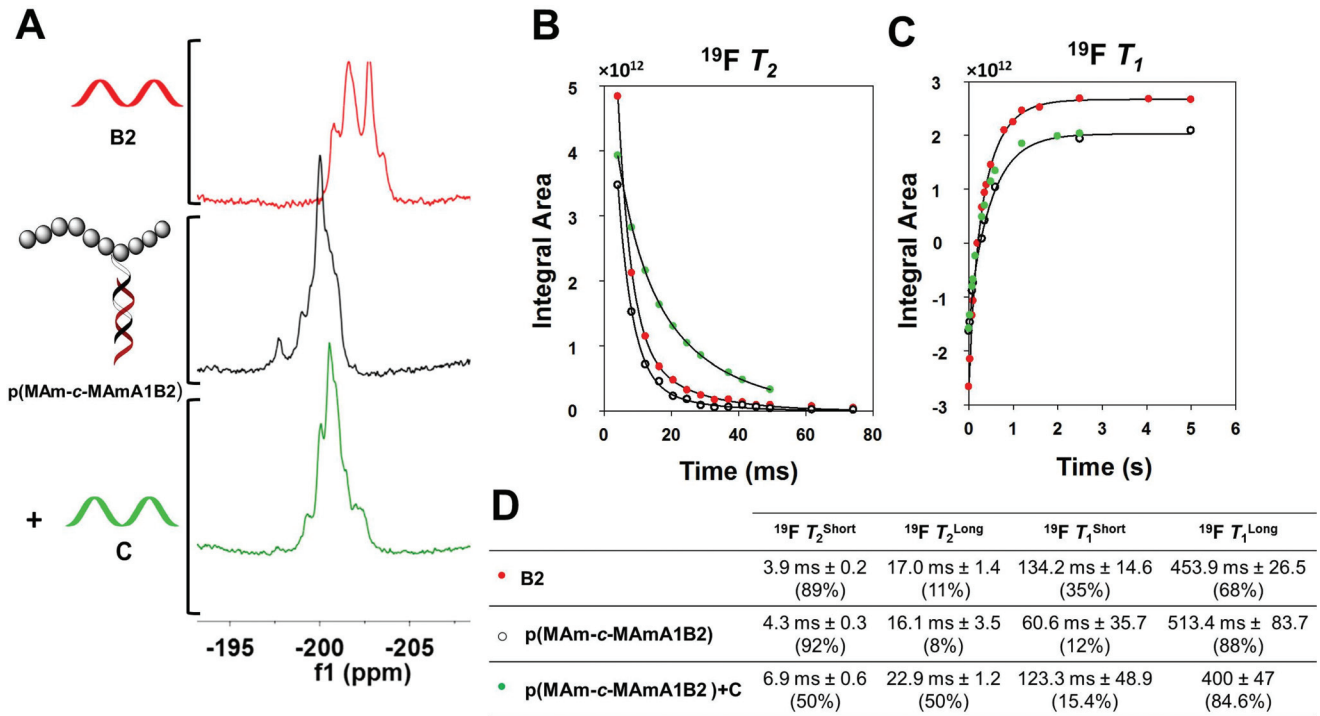


D

| | $^{19}$F $T_2^{Short}$ | $^{19}$F $T_2^{Long}$ | $^{19}$F $T_1^{Short}$ | $^{19}$F $T_1^{Long}$ |
|---|---|---|---|---|
| • B2 | 3.9 ms ± 0.2 (89%) | 17.0 ms ± 1.4 (11%) | 134.2 ms ± 14.6 (35%) | 453.9 ms ± 26.5 (68%) |
| ○ p(MAm-*c*-MAmA1B2) | 4.3 ms ± 0.3 (92%) | 16.1 ms ± 3.5 (8%) | 60.6 ms ± 35.7 (12%) | 513.4 ms ± 83.7 (88%) |
| • p(MAm-*c*-MAmA1B2)+C | 6.9 ms ± 0.6 (50%) | 22.9 ms ± 1.2 (50%) | 123.3 ms ± 48.9 (15.4%) | 400 ± 47 (84.6%) |

**Fig. 3** (A) 1D $^{19}$F NMR spectra of oligonucleotide B2 (red), p(MAm-*c*-MAmA1B2) (black) and p(MAm-*c*-MamA1B2) + C (green). (B) $^{19}$F $T_2$ and (C) $^{19}$F $T_1$ relaxation times measurements for oligonucleotide B2 (red filled circles), p(MAm-*c*-MAmA1B2) (black open circles) and p(Mam-*c*-MAmA1B2)+C (green filled circles) fitted with biexponential decay curves. (D) List of short and long $^{19}$F $T_2$ and $^{19}$F $T_1$ relaxation times with relative standard errors. The percentage of $^{19}$F spins displaying short and long relaxation times is reported in brackets.

causing a decrease of ~580 ms and ~ 330 ms of $T_1$ for proton resonating at 8.5–7.6 ppm and 6.4–5.5 ppm respectively.

### $^1$H and $^{19}$F self-diffusion coefficients of p(MAm-c-MAmA1B2)

Protons belonging either to the oligonucleotide nucleobases and the methylene side chains of the hybrid p(MAm-*c*-MAmA1B2) displayed similar self-diffusion coefficients in the range of $5.1 \times 10^{-10}$ m$^2$ s$^{-1}$ (Fig. S15†). As shown by the 2D $^1$H DOSY spectrum reported in Fig. 4A, the hybridised copolymer diffused at the same rate as the polymeric platform p(MAm-*c*-MAmA1) and approximately 10 times slower than the B2 strand. These data confirmed the success of the hybridization process. Traces of unbound strand B2 observed in the PAGE analysis could not be detected in the 2D DOSY experiments due to their low abundance.

Although the $^{19}$F spins seemed to diffuse at the same rate as the protons with a self-diffusion coefficient of $5.6 \times 10^{-10}$ m$^2$ s$^{-1}$, the $^{19}$F DOSY measurements resulted in a poor curve fitting (Fig. S16B†) due to significant loss of signal intensity during the analysis. As shown in Fig. 4C, the 1D $^{19}$F NMR of p(MAm-*c*-MAmA1B2) recorded after the 1$^{st}$ pulse gradient was characterised by a low intensity signal. In contrast, the strand B2 when free in solution exhibited a good signal to noise ratio after application of the 1$^{st}$ gradient pulse (Fig. 4B and Fig. S16A†). These results were as a consequence of the change in $^{19}$F spin–lattice relaxation times induced by the

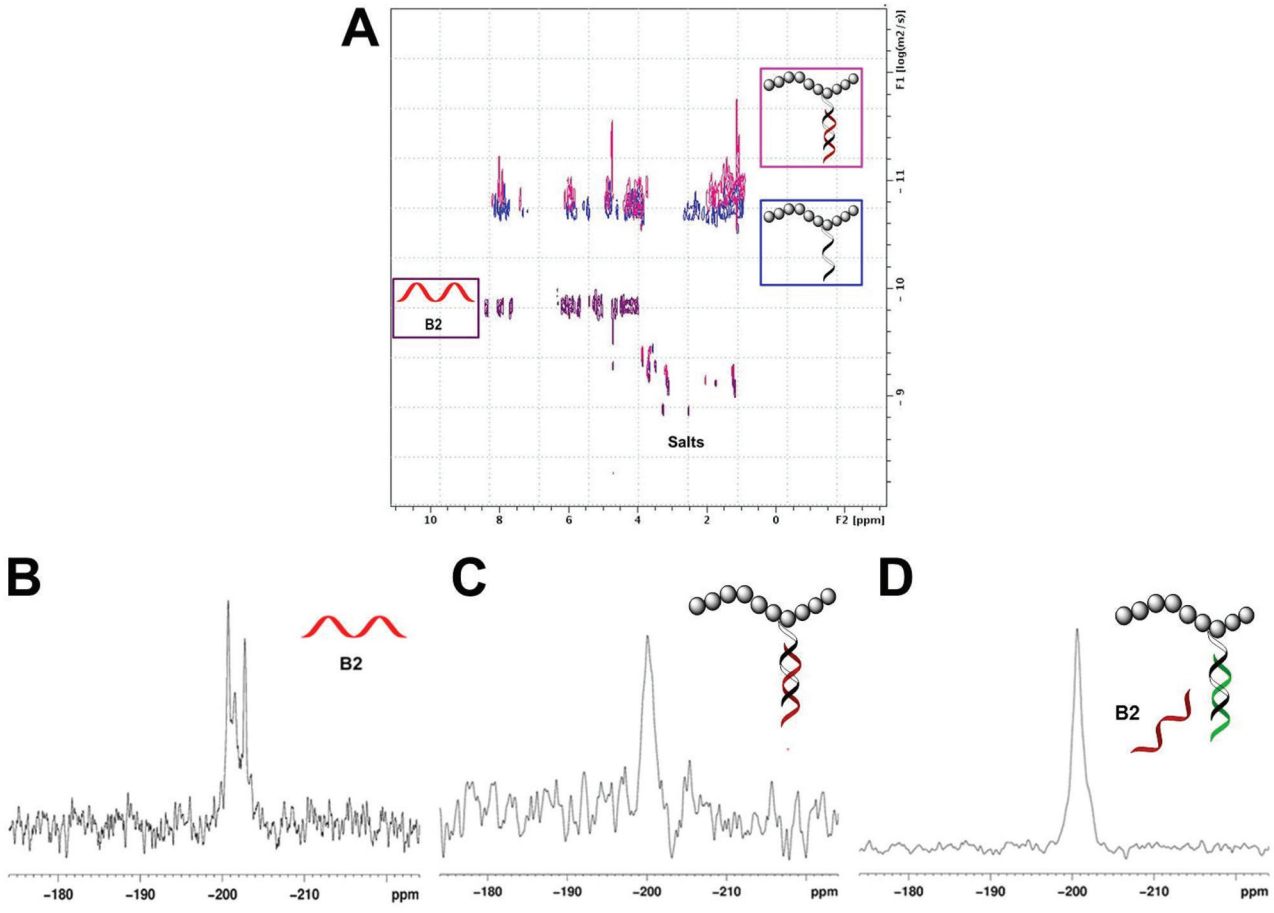


E

| | ppm | $^{19}$F Diffusion Coeff. (m$^2$s$^{-1}$) |
|---|---|---|
| ● B2 | -200.2 to -203.3 | (5.2 ± 0.4)*10$^{-9}$ |
| ○ p(MAm-*c*-MAmA1B2) | -199.6 to -200.6 | (5.6 ± 1.3)*10$^{-10}$ |
| ● p(MAm-*c*-MAmA1B2)+C | -198.6 to -202.8 | (2.3 ± 0.3)*10$^{-9}$ |

**Fig. 4** (A) 2D $^1$H DOSY overlap spectra of oligonucleotide B2 (purple), p(MAm-*c*-MAmA1) (blue) and p(MAm-*c*-MAmA1B2) (pink). 1D $^{19}$F spectrum acquired after 1$^{st}$ gradient pulse of (B) oligonucleotide B2, (C) p(MAm-*c*-MAmA1B2) and (D) p(MAm-*c*-MAmA1B2) + C. The negative logarithm of the area of the $^{19}$F signal detected for (E) oligonucleotide B2, (F) p(MAm-*c*-MAmA1B2) and (G) p(MAm-*c*-MAmA1B2) + C is plotted against the squared gradient strength. (H) List of $^{19}$F self-diffusion coefficients with relative standard errors.

 

hybridization of the fluorinated probe B2 to the polymer p(MAm-*c*-MAmA1). Fluorine self-diffusion coefficients were measured using the bipolar pulse pair longitudinal eddy current delay sequence (BPP-LED)[34] which has a strong dependence on longitudinal relaxation ($T_1$). As described by Claridge *et al.*,[31] signal losses generally occur in the presence of slow longitudinal relaxation rates. Here, the hybrid p(MAm-*c*-MAmA1B2) displayed longer $T_1$ relaxation times ($^{19}$F $T_1^{Long}$ = 513.4 ms; 88%) than the oligonucleotide B2 ($^{19}$F $T_1^{Long}$ = 453.9 ms; 68%) that lead to signal loss during the DOSY acquisition. Nonetheless, the DOSY data clearly showed the potential of this technique for monitoring hybridization and strand displacement in this system.

### Strand displacement of p(MAm-*c*-MAmA1B2)

The ability of a target DNA strand C to displace the fluorinated probe B2 from the hybrid p(MAm-*c*-MAmA1B2) could not be evaluated by gel electrophoresis because the bands corresponding to the fluorinated probe B2 and the target sequence C migrated at the same rate (Fig. S17†). Therefore, the hybrid p(MAm-*c*-MAmA1B2) was analysed by both $^1$H and $^{19}$F NMR after 30 minutes incubation at room temperature with 1 molar equivalent of oligonucleotide C. The interpretation of $^1$H $T_2$, $T_1$ relaxation times (Fig. S18†) and self-diffusion coefficients (Fig. S19†) measured for the oligonucleotide protons resonating at 8.5–7.6 ppm and 6.4–5.5 ppm was experimentally complex as these regions contained overlapping signals from a mixture of oligonucleotide strands such as B2, A1 and C. Therefore, the relaxation and diffusion coefficients observed for the oligonucleotide protons were average values reflecting the molecular mobility of both single and double stranded oligonucleotide species.

In contrast, $^{19}$F spin echo and DOSY experiments provided the possibility to monitor the effects that the incubation of the hybrid p(MAm-*c*-MAmA1) with the target DNA sequence C had on the molecular mobility of the fluorinated probe B2 only. By comparison with the hybrid p(MAm-*c*-MAmA1B2), the addition of strand C significantly altered the peak shape of the fluorine signal (Fig. 3A, green trace), increased the percentage (Fig. 3B–D) of fluorine spins experiencing longer transverse relaxation times (23 ms) from 8% to 50% and, importantly, promoted faster longitudinal relaxation. The long $^{19}$F $T_1$ component observed for the hybrid p(MAm-*c*-MAmA1B2) decreased from 513.4 ms to 400 ms after addition of the target sequence C. These changes in fluorine relaxivity were indicative of an increase in the molecular mobility of B2 following displacement.

As shown in Fig. 4E, the fluorinated probe B2 was found to diffuse 4 times faster than when bound to the hybrid p(MAm-

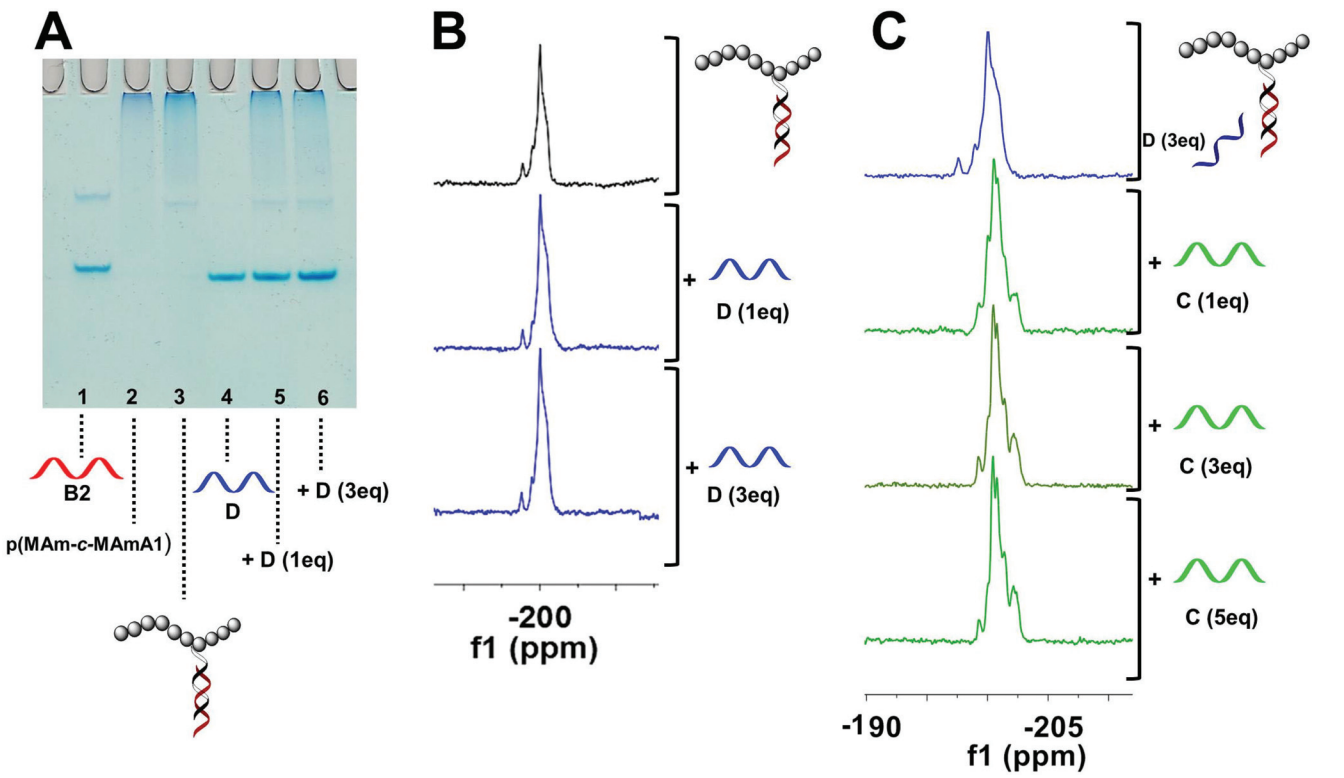


**Fig. 5** (A) 30% native PAGE testing the strand displacement process in presence of a non-specific DNA strand D. Lanes: 1. B2, 2. p(MAm-*c*-MAmA1), 3. p(MAm-*c*-MAmA1B2) (1 : 1.3), 4. D, 5. p(MAm-*c*-MAmA1B2)D (1 : 1.3 : 1), 6. p(MAm-*c*-MAmA1B2)D (1 : 1.3 : 2). (B) Stacked plot of 1D $^{19}$F NMR spectra of p(MAm-*c*-MAmA1B2) (black), p(MAm-*c*-MAmA1B2) after 30 min from the addition of 1 eq. and 3 eq. of strand D respectively (blue). (C) Stacked plot of 1D $^{19}$F NMR spectra of p(MAm-*c*-MAmA1B2) recorded after 30 min from the addition of D (3 eq.) (blue) and subsequent treatment with increasing amount of strand C (green).

*c*-MAmA1B2). Therefore, the fluorine Spin Echo and DOSY data strongly suggested that the target sequence C was able to displace the fluorinated probe from the polymeric platform p(MAm-*c*-MAmA1). However, the fact that the strand B2 did not (re)gain exactly the same mobility as when it was fully free in solution, can be inferred to either temporary interactions between the displaced strand B2 and the oligonucleotide species present in solution or to a partial displacement of the fluorinated probe. While this last hypothesis could have been probed further by incubating the hybrid p(MAm-*c*-MAmA1B2) with a larger excess of strand C, this experiment was not performed due to the expected increase in sample viscosity induced by the high DNA concentration that could affect spin echo and DOSY experiments. Finally, the decrease of $^{19}$F $T_1$ registered upon addition of the strand C, improved the intensity of the $^{19}$F signal during DOSY acquisition (Fig. 4D and Fig. S16C†). As shown in Fig. 4B–D, the changes in $^{19}$F $T_1$ observed for the hybrid p(MAm-*c*-MAmA1B2) before and after addition of the target DNA sequence C, constituted an apparent "off–on" signal switch during the DOSY experiments. These data accordingly showed the efficacy of the DOSY technique in probing nucleic acid binding and recognition events.

### Targeting strand selectivity of p(MAm-*c*-MAmA1B2)

In order to prove the ability of p(Mm-*c*-MAmA1B2) to respond only to target oligonucleotides, the hybrid p(MAm-*c*-MAmA1B2) was incubated with increasing concentration of a non-specific DNA sequence D of the same length as the target DNA strand C (Table 1). The strand selectivity of p(MAm-*c*-MAmA1B2) was monitored by PAGE and $^{19}$F NMR.

In contrast to what was observed for oligonucleotide C, the non-specific sequence D and the fluorine labelled probe B2 were characterised by a different electrophoretic mobility that enabled the investigation of strand selectivity by native PAGE. As shown in Fig. 5A, any traces of single stranded B2 could be clearly detected in the hybrids p(MAm-*c*-MAmA1B2) incubated with either 1 or 2 molar equivalent of D (Fig. 5A, lanes 5 and 6). The PAGE analysis thus indicated that the strand D was incapable of displacing the fluorinated probe from the hybrid p(MAm-*c*-MAmA1B2). These results were further confirmed by $^{19}$F NMR. As shown in Fig. 5B (blue traces), the addition of increasing amount of strand D to the hybrid p(MAm-*c*-MAmA1B2) did not cause any significant change to either the fluorine signal shape and chemical shift.

In order to prove the capability of p(MAm-*c*-MAmA1B2) to respond only to target sequences even when surrounded by a pool of non-specific oligonucleotides (in this case, strand D), the hybrid p(MAm-*c*-MAmA1B2) was titrated with increasing amounts of target DNA C after being incubated initially with 3 molar equivalents of strand D. As shown in Fig. 5C (green traces), the addition of strand D had a minimal effect on the $^{19}$F spectrum, while the addition of C had an immediate effect on the fluorine signal shape. Therefore, this experiment provided evidence that the polymer nucleic acid conjugates respond selectively to target oligonucleotide strands and more importantly the ability of $^{19}$F NMR spectroscopy to probe nucleic acid binding events even in complex mixtures (Fig. 5C).

## Conclusions

In this work, the synthesis of a novel 2′-fluoro modified nucleic acid-polymer conjugate p(MAm-*c*-MAmA1B2) was described. Furthermore, the capability of the hybrid conjugate to bind to target oligonucleotide sequences was demonstrated *via* 2D Spin Echo and DOSY $^{19}$F NMR spectroscopy.

An in depth analysis on the effects that nucleic acid binding events have on fluorine relaxation and diffusivity was carried out on the hybrid p(MAm-*c*-MAmA1B2) before and after incubation with specific and non-specific DNA strands. The binding to target DNA sequences occurring *via* toehold mediated strand displacement process was demonstrated to alter significantly the relaxivity and diffusivity of the fluorine labelled oligonucleotide probe B2. These alterations resulted in measurable $^{19}$F $T_2$ and $T_1$ relaxation times and self-diffusion coefficients. On the basis of the $^{19}$F Spin Echo and DOSY NMR results obtained, it is reasonable to suggest that the 2′-fluoro modified nucleic acid–polymer conjugate p(MAm-*c*-MAmA1B2) has some potential as an *in vitro* NMR reporter of nucleic acids recognition and binding events, but limited applicability as *in vivo* imaging agent due to the low sensitivity of the magnetic resonance imaging technique to fast fluorine transverse relaxation.

The fluorine signal to noise ratio can be improved either by increasing the number of scans or the concentration of the fluorine labelled oligonucleotide probes. Unfortunately, the first approach requires long acquisition times and the second evokes cost penalties. Nonetheless, this report provides a potential route towards developing diagnostic probes for DNA strand displacement by $^{19}$F NMR. Importantly, the high sensitivity of the $^{19}$F nuclei to local environment provides a very powerful technique for monitoring subtle changes in the displacement reaction and hence enables *in situ* observation of dynamic processes. This could be utilised in both *in vitro* and *in vivo* diagnostics and provides advantages over traditional FRET approaches. The FRET method can require complex probe design and is often characterized by poor conjugation efficiency of the FRET pair to oligonucleotide sequences. Importantly, when applied to *in vivo* diagnostics, FRET methods suffer from low tissue penetration depths (<1 cm) which lead to poor spatial resolution images. Accordingly, the use of fluorine NMR probes offers the possibility to observe biomolecule binding phenomena in complex solutions and in tissue environments where specific disease markers may otherwise be undetectable.

## Acknowledgements

We thank the UK EPSRC (Grants EP/H005625/1, EP/G042462/1) and the University of Nottingham for a Scholarship (GS).

 

KJT acknowledges the Australian Research Council for funding (FT110100284, DP140100951) and is part of the Centre of Excellence in Convergent BioNano Science and Technology (CE140100036). We also thank Professor Chris Hayes (School of Chemistry, University of Nottingham) for assistance with DNA modification and Christine Grainger-Boultby, Tom Booth and Paul Cooling for technical support.

## Notes and references

1 M. Ye, J. Guillaume, Y. Liu, R. Sha, R. Wang, N. C. Seeman and J. W. Canary, *Chem. Sci.*, 2013, **4**, 1319–1329.
2 C. K. McLaughlin, G. D. Hamblin and H. F. Sleiman, *Chem. Soc. Rev.*, 2011, **40**, 5647–5656.
3 S. M. Douglas, H. Dietz, T. Liedl, B. Hogberg, F. Graf and W. M. Shih, *Nature*, 2009, **459**, 414–418.
4 E. S. Andersen, M. Dong, M. M. Nielsen, K. Jahn, R. Subramani, W. Mamdouh, M. M. Golas, B. Sander, H. Stark, C. L. P. Oliveira, J. S. Pedersen, V. Birkedal, F. Besenbacher, K. V. Gothelf and J. Kjems, *Nature*, 2009, **459**, 73–76.
5 M. Endo, Y. Yang and H. Sugiyama, *Biomater. Sci.*, 2013, **1**, 347–360.
6 G. Zhang, S. P. Surwade, F. Zhou and H. Liu, *Chem. Soc. Rev.*, 2013, **42**, 2488–2496.
7 B. Chakraborty, N. Jonoska and N. C. Seeman, *Chem. Sci.*, 2012, **3**, 168–176.
8 P. J. Milnes, M. L. McKee, J. Bath, L. Song, E. Stulz, A. J. Turberfield and R. K. O'Reilly, *Chem. Commun.*, 2012, **48**, 5614–5616.
9 Y.-X. Zhao, A. Shaw, X. Zeng, E. Benson, A. M. Nystrom and B. Hogberg, *ACS Nano*, 2012, **6**, 8684–8691.
10 G. Yasayan, J. P. Magnusson, G. Sicilia, S. G. Spain, S. Allen, M. C. Davies and C. Alexander, *Phys. Chem. Chem. Phys.*, 2013, **15**, 16263–16274.
11 G. Sicilia, C. Grainger-Boultby, N. Francini, J. P. Magnusson, A. O. Saeed, F. Fernandez-Trillo, S. G. Spain and C. Alexander, *Biomater. Sci.*, 2014, **2**, 203–211.
12 Y. Murakami and M. Maeda, *Biomacromolecules*, 2005, **6**, 2927–2929.
13 E. D. Goluch, J. M. Nam, D. G. Georganopoulou, T. N. Chiesl, K. A. Shaikh, K. S. Ryu, A. E. Barron, C. A. Mirkin and C. Liu, *Lab Chip*, 2006, **6**, 1293–1299.
14 K. J. Watson, S. J. Park, J. H. Im, S. T. Nguyen and C. A. Mirkin, *J. Am. Chem. Soc.*, 2001, **123**, 5592–5593.
15 J. P. Magnusson, F. Fernandez-Trillo, G. Sicilia, S. G. Spain and C. Alexander, *Nanoscale*, 2014, **6**, 2368–2374.
16 L. Josephson, J. M. Perez and R. Weissleder, *Angew. Chem., Int. Ed.*, 2001, **40**, 3204–3206.
17 J. M. Perez, L. Josephson and R. Weissleder, *ChemBioChem*, 2004, **5**, 261–264.
18 P. Liu, A. Sharon and C. K. Chu, *J. Fluorine Chem.*, 2008, **129**, 743–766.
19 S. D. Warren, *J. Med. Chem.*, 2009, **52**, 6503–6503.
20 B. E. Rolfe, I. Blakey, O. Squires, H. Peng, N. R. B. Boase, C. Alexander, P. G. Parsons, G. M. Boyle, A. K. Whittaker and K. J. Thurecht, *J. Am. Chem. Soc.*, 2014, **136**, 2413–2419.
21 M. Ogawa, S. Nitahara, H. Aoki, S. Ito, M. Narazaki and T. Matsuda, *Macromol. Chem. Phys.*, 2010, **211**, 1602–1609.
22 K. W. Pankiewicz, *Carbohydr. Res.*, 2000, **327**, 87–105.
23 M. Olejniczak, Z. Gdaniec, A. Fischer, T. Grabarkiewicz, Ł. Bielecki and R. W. Adamiak, *Nucleic Acids Res.*, 2002, **30**, 4241–4249.
24 J. C. Penedo, T. J. Wilson, S. D. Jayasena, A. Khvorova and D. M. J. Lilley, *RNA*, 2004, **10**, 880–888.
25 J. R. P. Arnold and J. Fisher, *J. Biomol. Struct. Dyn.*, 2000, **17**, 843–856.
26 A. Kieger, M. J. Wiester, D. Procissi, T. B. Parrish, C. A. Mirkin and C. S. Thaxton, *Small*, 2011, **7**, 1977–1981.
27 M. J. Damha, C. J. Wilds, A. Noronha, I. Brukner, G. Borkow, D. Arion and M. A. Parniak, *J. Am. Chem. Soc.*, 1998, **120**, 12976–12977.
28 T. Dowler, D. Bergeron, A.-L. Tedeschi, L. Paquet, N. Ferrari and M. J. Damha, *Nucleic Acids Res.*, 2006, **34**, 1669–1675.
29 S. L. Beaucage and M. H. Caruthers, *Tetrahedron Lett.*, 1981, **22**, 1859–1862.
30 F. Wüthrich, *NMR of Proteins and Nucleic Acids*, 1st Edition edn, 1986.
31 T. D. W. Claridge, in *Tetrahedron Organic Chemistry Series*, ed. D. W. C. Timothy, Elsevier, 2009, vol. 27, pp. 11–34.
32 S. Z. Mao, X. D. Zhang, J. M. Dereppe and Y. R. Du, *Colloid Polym. Sci.*, 2000, **278**, 264–269.
33 G. Wider, *J. Magn. Reson., Ser. A*, 1994, **108**, 255–258.
34 D. H. Wu, A. D. Chen and C. S. Johnson, *J. Magn. Reson., Ser. A*, 1995, **115**, 260–264.
35 S. J. Gibbs and C. S. Johnson Jr., *J. Magn. Reson.*, 1991, **93**, 395–402.
36 H. Peng, I. Blakey, B. Dargaville, F. Rasoul, S. Rose and A. K. Whittaker, *Biomacromolecules*, 2009, **10**, 374–381.
37 L. Nurmi, H. Peng, J. Seppala, D. M. Haddleton, I. Blakey and A. K. Whittaker, *Polym. Chem.*, 2010, **1**, 1039–1047.
38 J. F. Parsons, G. Xiao, G. L. Gilliland and R. N. Armstrong, *Biochemistry*, 1998, **37**, 6286–6294.
39 G. Xiao, J. F. Parsons, K. Tesh, R. N. Armstrong and G. L. Gilliland, *J. Mol. Biol.*, 1998, **281**, 323–339.
40 R. E. Hendrick, *Magn. Reson. Imaging*, 1987, **5**, 31–37.
41 R. E. Banks and J. C. Tatlow, *J. Fluorine Chem.*, 1986, **33**, 227–346.
42 A. Kiviniemi, M. Murtola, P. Ingman and P. Virta, *J. Org. Chem.*, 2013, **78**, 5153–5159.